

1 **Title:**

2 **Near-infrared imaging in fission yeast by genetically encoded biosynthesis of phycocyanobilin**

3

4 **Running Title:**

5 **iRFP imaging in fission yeast**

6

7 **Authors:**

8 Keiichiro Sakai,^{1,2,3} Yohei Kondo,^{1,2,3} Hiroyoshi Fujioka,⁴ Mako Kamiya,⁵ Kazuhiro Aoki,^{1,2,3,*} and
9 Yuhei Goto,^{1,2,3*}

10

11 **Affiliations:**

12 ¹Quantitative Biology Research Group, Exploratory Research Center on Life and Living Systems
13 (ExCELLS), National Institutes of Natural Sciences, 5-1 Higashiyama, Myodaiji-cho, Okazaki, Aichi
14 444-8787, Japan.

15 ²Division of Quantitative Biology, National Institute for Basic Biology, National Institutes of Natural
16 Sciences, 5-1 Higashiyama, Myodaiji-cho, Okazaki, Aichi 444-8787, Japan.

17 ³Department of Basic Biology, School of Life Science, SOKENDAI (The Graduate University for
18 Advanced Studies), 5-1 Higashiyama, Myodaiji-cho, Okazaki, Aichi 444-8787, Japan.

19 ⁴Graduate School of Pharmaceutical Sciences, The University of Tokyo, 7-3-1 Hongo, Bunkyo-ku,
20 Tokyo 113-0033, Japan.

21 ⁵Graduate School of Medicine, The University of Tokyo, 7-3-1 Hongo, Bunkyo-ku, Tokyo 113-0033,
22 Japan

23 *Correspondence author

24

25 **Contact information:**

26 k-aoki@nibb.ac.jp, y-goto@nibb.ac.jp

27

28 **KEYWORDS:**

29 fission yeast, iRFP, biliverdin, phycocyanobilin, imaging

30

31 **ABSTRACT**

32 Near-infrared fluorescent protein (iRFP) is the bright and stable fluorescent protein with excitation and
33 emission maxima at 690 nm and 713 nm, respectively. Unlike the other conventional fluorescent
34 proteins such as GFP, iRFP requires biliverdin (BV) as a chromophore because iRFP originates from
35 phytochrome. Here, we report that phycocyanobilin (PCB) functions as a brighter chromophore for
36 iRFP than BV, and biosynthesis of PCB allows live-cell imaging with iRFP in fission yeast
37 *Schizosaccharomyces pombe*. We initially found that fission yeast cells did not produce BV, and
38 therefore did not show any iRFP fluorescence. The brightness of iRFP attached to PCB was higher than
39 that attached to BV *in vitro* and in fission yeast. We introduced SynPCB, a previously reported PCB
40 biosynthesis system, into fission yeast, resulting in the brightest iRFP fluorescence. To make iRFP
41 readily available in fission yeast, we developed an endogenous gene tagging system with iRFP and all-
42 in-one integration plasmids, which contain genes required for the SynPCB system and the iRFP-fused
43 marker proteins. These tools not only enable the easy use of iRFP in fission yeast and the multiplexed
44 live-cell imaging in fission yeast with a broader color palette, but also open the doors to new
45 opportunities for near-infrared fluorescence imaging in a wider range of living organisms.

46

47

48 INTRODUCTION

49

50 Fluorescent proteins (FPs) have become indispensable to visualize the biological processes in living
51 cells and tissues (Lambert, 2019). Green fluorescent protein (GFP), the most widely used FP, has been
52 intensively modified to improve the brightness, photo-, thermo-, pH-stabilities, and change the
53 excitation and emission spectrum. A variety of fluorescent proteins with different excitation and
54 emission spectra enable the multiplexed fluorescence imaging to monitor the multiple biological events
55 simultaneously at high spatial and temporal resolution.

56 Near-infrared fluorescent proteins have been developed through engineering phytochromes,
57 which are photosensory proteins of plants, bacteria, and fungi (Chernov et al., 2017). RpBphP2 from
58 photosynthetic bacteria has been engineered as iRFP (later renamed iRFP713) by the truncation and the
59 saturation mutagenesis (Filonov et al., 2011). Following the report of iRFP, enormous efforts have been
60 devoted to developing near-infrared FPs with higher brightness, monomer formation, and longer
61 wavelength (Filonov et al., 2011; Fushimi et al., 2019; Kamper et al., 2018; Matlashov et al., 2020;
62 Oliinyk et al., 2019; Rodriguez et al., 2016; Rogers et al., 2019; Shcherbakova and Verkhusha, 2013;
63 Shcherbakova et al., 2016; Shcherbakova et al., 2018; Stepanenko et al., 2016; Yu et al., 2014; Yu et
64 al., 2015). Unlike the canonical fluorescent proteins derived from jellyfish or coral, phytochromes
65 require a linear tetrapyrrole as a chromophore such as biliverdin IX α (BV), phycocyanobilin (PCB),
66 and phytochromobilin (P Φ B), and autocatalytically forms a covalent bond with a chromophore
67 (Fushimi and Narikawa, 2021). These linear tetrapyrroles are produced from heme. Heme-oxygenase
68 (HO) catalyzes oxidative cleavage of heme to generate BV with the help of ferredoxin (Fd), an electron
69 donor, and ferredoxin-NADP⁺ reductase (Fnr). In cyanobacteria, PCB is produced from BV through
70 PcyA, Fd, and Fnr, while in higher plants P Φ B is synthesized from BV using HY2, Fd, and Fnr. To
71 exploit phytochromes that are required for PCB or P Φ B in other organisms, our group and others have
72 demonstrated reconstitution of BV, PCB, and P Φ B synthesis in bacteria, mammalian cells, frog egg,
73 budding yeast, *Pichia*, and fission yeast (Gambetta and Lagarias, 2001; Hochrein et al., 2017;
74 Kyriakakis et al., 2018; Landgraf et al., 2001; Mukougawa et al., 2006; Müller et al., 2013; Shin et al.,
75 2014; Tooley et al., 2001; Uda et al., 2017).

76 As the fluorescence of iRFP depends on the chromophore formation, BV concentration is of
77 critical importance for imaging iRFP (Fig. 1A). Indeed, it has been reported that the addition of
78 purified BV increases the fluorescence of iRFPs (Piatkevich et al., 2017; Shemetov et al., 2017).
79 Alternatively, genetic modifications such as the overexpression of HO1), which catalyzes heme to

80 generate BV, and the knocked out of biliverdin reductase A (BVRA), which degrades BV to generate
81 bilirubin, improves the brightness of iRFP through the additional accumulation of BV (Kobachi et al.,
82 2020; Shemetov et al., 2017). On the other hand, because *Caenorhabditis elegans* can hardly produce
83 BV (Ding et al., 2017), it is incapable of imaging iRFP by simply introducing only the iRFP gene in
84 nematodes. In the case of multicellular organisms that cannot produce BV such as nematodes, the
85 introduction of genes required for BV production is more effective than the external addition of BV,
86 because of the low tissue penetration property. However, at present, only the introduction of the HO1
87 gene has been reported as a genetically encoded method for inducing the iRFP chromophore, and it has
88 not been improved or optimized yet.

89 Here, we report that PCB acts as a better chromophore for iRFP than BV, and genetically
90 encoded PCB synthesis outperforms HO1-mediated BV production in terms of iRFP brightness in
91 fission yeast. We accidentally found that iRFP did not fluoresce in fission yeast because of the lack of
92 HO1 gene, and therefore the lack of BV. Both the external BV addition and heterologous HO1
93 expression renders iRFP fluorescent in fission yeast. To our surprise, PCB biosynthesis with SynPCB
94 system, which we have previously reported (Uda et al., 2017; Uda et al., 2020), and treatment of
95 purified PCB demonstrated brighter iRFP fluorescence than iRFP fluorescence with BV biosynthesis or
96 the treatment. We confirmed that PCB-bound iRFP showed higher fluorescence quantum yield than
97 BV-bound iRFP. To facilitate the simple use of iRFP in fission yeast, we developed an endogenous
98 tagging plasmid at the C-terminus with iRFP, novel genome integration vectors, and all-in-one
99 plasmids carrying genes required for both SynPCB system and iRFP-fused marker proteins.

100

101

102

103

104 **RESULTS**

105
106 **iRFP does not fluoresce in fission yeast *Schizosaccharomyces pombe***

107 We accidentally found that iRFP did not fluoresce at all in fission yeast during the process of
108 experiments. Firstly, to test whether iRFP was applicable to near- infrared imaging in fission yeast, we
109 established a cell strain stably expressing nuclear localization signal (NLS)-iRFP-NLS under
110 constitutive promoter *Padh1*. No iRFP fluorescence was observed with excitation wavelength of 640
111 nm (Fig. 1B). Because the iRFP requires BV as a chromophore for emitting fluorescence (Fig. 1A), we
112 hypothesized that fission yeast could not metabolize BV within a cell. Upon the addition of external
113 BV, the nuclear iRFP fluorescence signal was recovered (Fig. 1B). The titration of BV concentration
114 yielded dose-dependent increase in iRFP fluorescence up to 125 μ M (Fig. 1C). We next examined the
115 kinetics of BV incorporation into fission yeast cells. High dose of BV (500 μ M) treatment gradually
116 increased iRFP fluorescence and reached a plateau at 60-120 min after the treatment (Fig. 1D). Since
117 BV is produced from heme through HO, we explored *HO* in the genomes of fission yeast and
118 representative fungal species. As expected, we could not find any *HO* and *HO*-like gene in fission yeast
119 (Fig. S1). Interestingly, *HO* and/or *HO*-like genes, which have been found from bacteria to higher
120 eukaryotes, are frequently and sporadically lost in the representative fungal species (Fig. S1). Indeed,
121 while iRFP has been widely used in budding yeast, *Saccharomyces cerevisiae*, which remains *HO* gene
122 (Geller et al., 2019; Li et al., 2017; Tojima et al., 2019; Wosika et al., 2016), there has been no reports
123 of using iRFP in fission yeast, *Schizosaccharomyces pombe*. Taken together, we concluded that iRFP
124 does not fluoresce in fission yeast because of the lack of BV and *HO*.

125
126
127
128
129
130
131
132
133
134
135

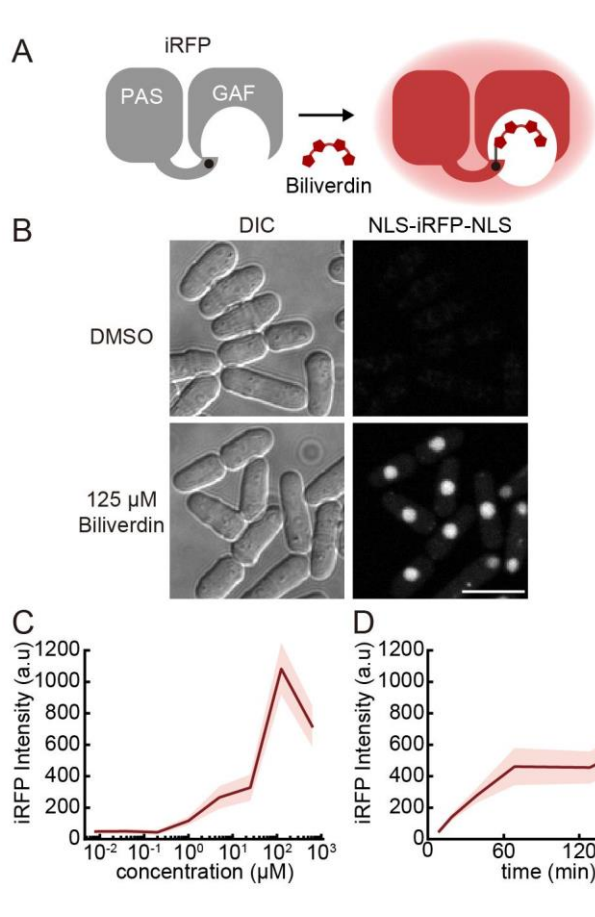


Fig 1. iRFP does not fluoresce in fission yeast.

(A) Schematic illustration of chromophore formation of iRFP with biliverdin (BV). BV covalently attaches to iRFP as a chromophore. The PAS domain in iRFP contains a conserved cysteine residue at the N-terminus that covalently attaches to the BV, while the BV itself fits into the cleft in the GAF domain. (B) Representative images of fission yeast expressing NLS-iRFP-NLS with or without external BV treatment. Scale bar, 10 μ m. (C) Dose-response of BV incorporation into fission yeast cells. Fission yeast cells were cultured in liquid YEA and incubated at room temperature for 3 h with the indicated concentration of BV (8 nM, 40 nM, 200 nM, 1 μ M, 5 μ M, 25 μ M, 125 μ M, and 625 μ M). The red line and shaded area indicate the averaged intensity and S.D., respectively (n = 50 cells). (D) Time-course of BV incorporation into fission yeast cells. Fission yeast cells were cultured in liquid YEA and treated with 500 μ M BV at the time zero. The red line and shaded area indicate the averaged intensity and S.D., respectively (n = 50 cells).

161

162 Development of novel stable knock-in plasmids: pSKI

163 The above results showed that the external supply of BV required high dose and long-term incubation
164 (60-120 min) for iRFP fluorescence in fission yeast, prompting us to introduce genes for iRFP's
165 chromophore biosynthesis. Before starting to develop the reconstitution system, we developed novel
166 stable integration vectors, which satisfy our requirements; stable one copy integration into the genome,
167 no effect on the auxotrophy of integrated cells, and distant integration loci for crossing strains, although
168 several integration systems have been already developed (Fennessy et al., 2014; Kakui et al., 2015;
169 Keeney and Boeke, 1994; Matsuyama et al., 2004; Maundrell, 1993; Siam et al., 2004; Vještica et al.,
170 2020). At first, we chose three gene-free loci on each chromosome at chromosome I 1,508,522 to
171 1,508,641 (near *mug165*, 1L), chromosome II 447,732 to 447,827 (near *pho4*, 2L), and chromosome III
172 1,822,244 to 1,822,343 (near *nup60*, 3R) (Fig. S2A). Next, we designed and developed plasmids that
173 contain genes required for replication and amplification in *E. coli* (*Amp*, *ori*), constitutive promoter
174 *Padh1* or inducible one *Pnmt1*, multiple cloning site (MCS), *adh1* terminator, a selection marker
175 cassette encoding antibiotics resistant gene for fission yeast, and homology-arms connected with the

176 one-cut restriction enzyme recognition site for plasmid linearization (Fig. S2B). Expected genomic
177 integration with these vectors was confirmed by genomic PCR using primers designed to span the
178 integration boundary (Fig. S2C). None of these integrations affected bulk growth of fission yeast (Fig.
179 S2D), and the protein expression levels from these three loci were comparable or moderately higher
180 than that from Z-locus (Fig. S2E). We named these plasmid series as pSKI (p_lasmid for St_lable Knock-
181 In, also see Table S1) and used them for the following experiments.

182

183 **PCB brightens iRFP more efficiently than BV in fission yeast**

184 HO is the crucial enzyme in the BV biosynthesis pathway, catalyzing the linearization of tetrapyrrole
185 (Fig. 2A). Therefore, we established fission yeast cells stably expressing HO1 and NLS-iRFP-NLS
186 with pSKI, and quantified iRFP fluorescence. As expected, the expression of HO1 derived from
187 *Thermosynechococcus elongatus* BP-1 in mitochondria, where heme is abundant, demonstrated iRFP
188 fluorescence, and the iRFP fluorescence was brighter than that with the external addition of BV (Fig.
189 2B, second and third columns). HO1 is known to catalyze heme in the presence of reduced Fd (Rhie
190 and Beale, 1992), we next examined whether co-expression of HO1 and tFnr-Fd, a chimeric protein of
191 truncated Fnr and Fd (Uda et al., 2020), improved HO1-mediated iRFP fluorescence. However, the co-
192 expression of HO1 and tFnr-Fd in mitochondria did not further enhance iRFP fluorescence as
193 compared to the expression of only HO1 (Fig. 2B, sixth column), suggesting that authentic ferredoxin
194 in fission yeast sufficiently supports the catalytic reaction through HO1.

195 Unexpectedly, in a series of experiments, we found a further increment in iRFP fluorescence by
196 PCB (Fig. 2B, ninth column). PcyA, the enzyme responsible for the production of PCB from BV, HO1,
197 and tFnr-Fd, were co-expressed in mitochondria of fission yeast, showing the highest iRFP
198 fluorescence (Fig. 2B, ninth column). To validate these results, we treated the cells expressing NLS-
199 iRFP-NLS with purified PCB instead of BV. The addition of external PCB substantially outperformed
200 that of BV with respect to iRFP fluorescent intensity (Fig. 2C and 2D). While the fluorescence
201 intensities were quite different between PCB-bound iRFP (iRFP-PCB) and BV-bound iRFP (iRFP-
202 BV), effective concentration of dose response curve (Fig. 1C and 2C) and the kinetics of chromophore
203 incorporation (Fig. 1D and 2D) were comparable between them.

204

205

206

207

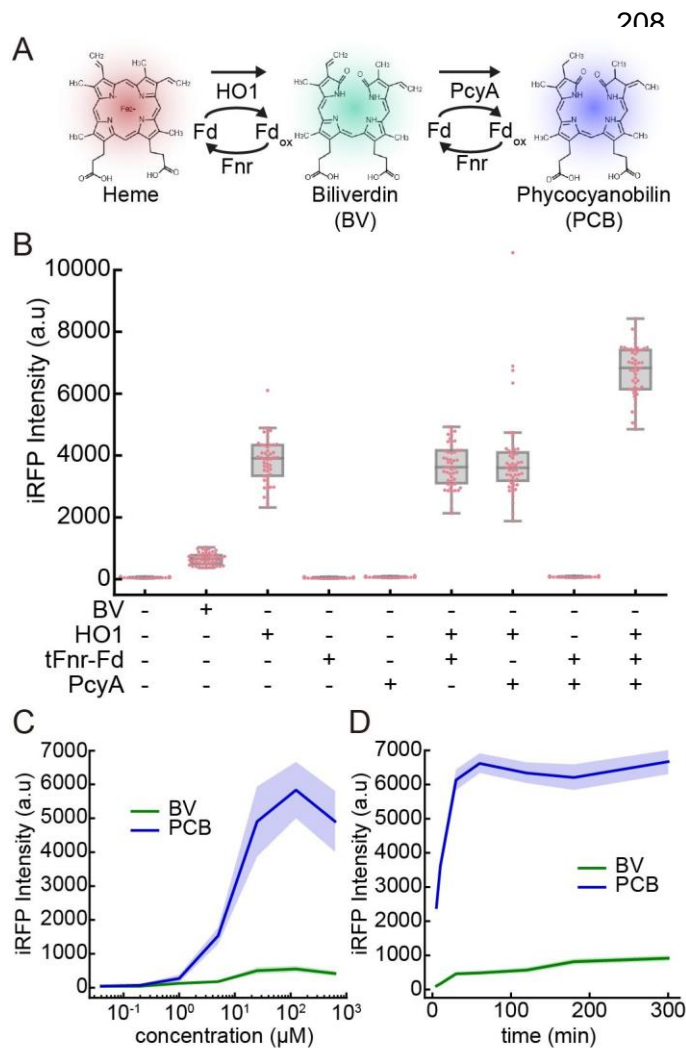


Fig 2. PCB brightens iRFP more efficiently than BV in fission yeast.

(A) Schematic illustration of PCB biosynthesis pathway. (B) Quantification of iRFP fluorescence in fission yeast cells expressing HO1, tFnr-Fd, and PcyA. Under the BV condition, cells were treated with 125 μM BV for 1 h at room temperature. Each dot represents a single cell iRFP fluorescence with a boxplot, in which the box shows the quartiles of data with the whiskers denoting the minimum and maximum except for the outliers detected by 1.5 times the interquartile range ($n = 50$ cells). (C) Dose-response of BV or PCB incorporation to iRFP fluorescence in fission yeast cells. Fission yeast cells were cultured in liquid YEA and incubated at room temperature for 3 h with the indicated concentration of BV or PCB (8 nM, 40 nM, 200 nM, 1 μM , 5 μM , 25 μM , 125 μM , and 625 μM). The lines and shaded areas indicate the averaged intensities and S.D., respectively ($n = 50$ cells). (D) Time-course of iRFP fluorescence in response to BV or PCB treatment. Fission yeast cells were cultured in liquid YEA and treated with 125 μM BV or PCB at zero. The lines and shaded areas indicate the averaged intensities and S.D., respectively ($n = 50$ cells).

237

238 **PCB is a brighter chromophore than BV for iRFP fluorescence**

239 The above data indicated the possibility that PCB might be a more suitable chromophore for iRFP than
 240 BV. To prove this hypothesis, we first examined whether the efficiency of holo-iRFP formation
 241 attributes the difference of iRFP fluorescence between BV- and PCB-treated cells. PCB was added to
 242 the cells with HO1 expression, in which BV was produced constantly within a cell. Therefore, iRFP
 243 has already formed a holo-complex with BV before attaching to PCB (Fig. 3A). Given that iRFP-PCB
 244 is brighter than iRFP-BV, HO1 expression attenuates the increase in iRFP fluorescence when purified
 245 PCB is further treated with the cells because of the competition in chromophore with already existing
 246 BV. As we expected, the addition of purified PCB hardly increased iRFP fluorescence in cells that had
 247 been expressing HO1, in spite of the dose-dependent increase in iRFP fluorescence by PCB treatment
 248 in cells not expressing HO1 (Fig. 3B and 3C). These observations point out that almost all iRFP forms
 249 holo-complex with BV when HO1 is expressed.

250 To understand why iRFP-PCB was brighter than iRFP-BV, we prepared recombinant iRFP
 251 expressed in *E. coli* and purified apo-iRFP (Filonov et al., 2011) (Fig. S3A). Apo-iRFP was mixed with
 252 PCB and BV to form holo-iRFP, *i.e.*, iRFP-PCB and iRFP-BV, respectively (Fig. S3B). Binding of
 253 PCB to iRFP resulted in the change in absorption spectrum from the free PCB (Fig. 3D). The
 254 absorbance maximum of iRFP-PCB was 10 nm blue-shifted from that of iRFP-BV (Fig. 3E).
 255 Fluorescence excitation and emission spectra were also 10 nm blue-shifted in iRFP-PCB compared to
 256 iRFP-BV (Fig. S3C and S3D). Notably, the fluorescence quantum yield of iRFP-PCB was nearly twice
 257 as high as that of iRFP-BV (0.094 vs. 0.054), while their molecular extinction coefficient values were
 258 comparable (Fig. 3F). Based on these results, we concluded that iRFP forms a complex with PCB as a
 259 holo-form and that iRFP-PCB is brighter than iRFP-BV at the molecular level.

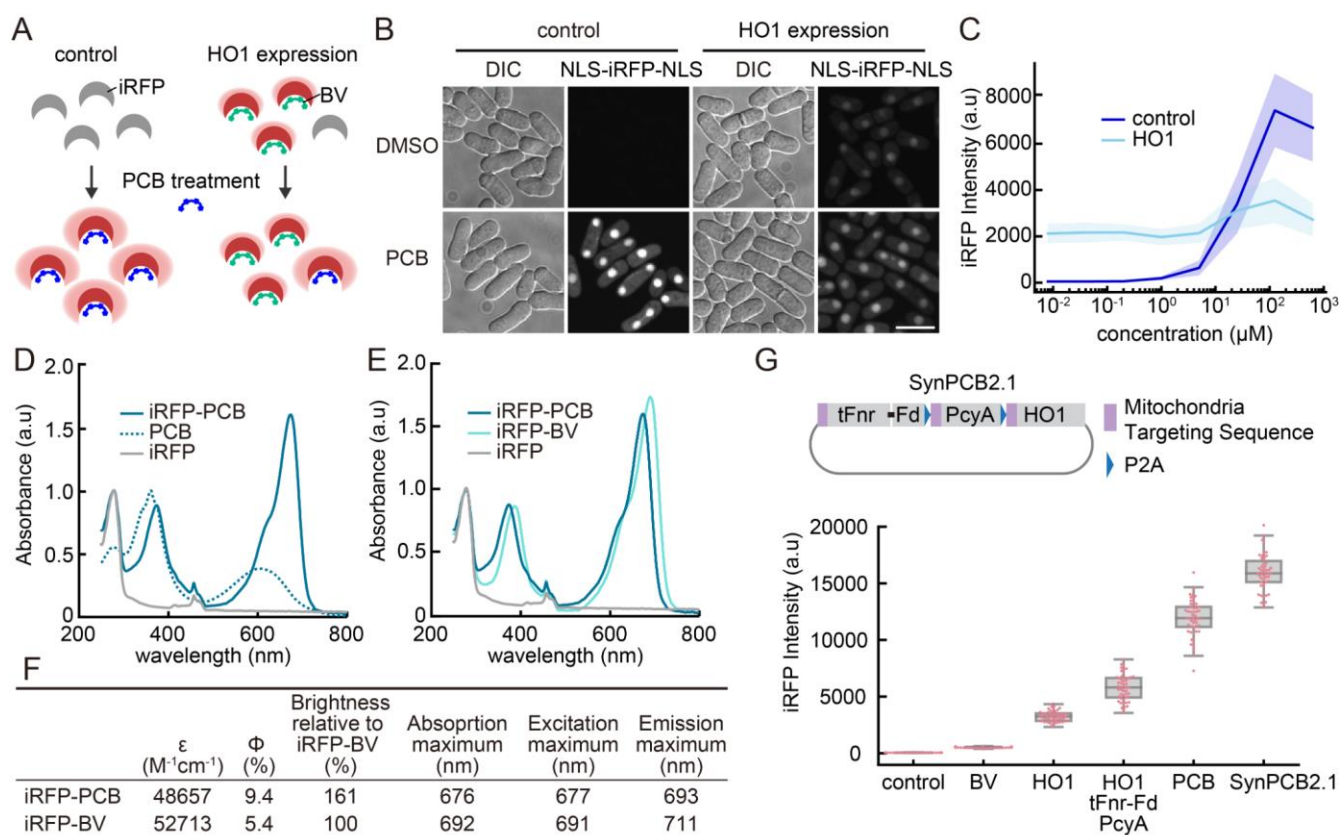


Fig 3. PCB is a brighter chromophore than BV for iRFP fluorescence

260
 261
 262 (A) Schematic illustration of the experimental procedure. In control fission yeast cells, iRFP shows
 263 fluorescence upon the addition of PCB. In HO1 expressing cells, BV binds to iRFP as a chromophore
 264 before the addition of PCB. Therefore, BV competes with the binding of PCB to iRFP. (B)
 265 Representative images of fission yeast expressing NLS-iRFP-NLS with or without external PCB (125
 266 μ M) treatment. Scale bar, 10 μ m. (C) Dose-response of PCB treatment to iRFP fluorescence in fission
 267 yeast cells with or without HO1 expression. Fission yeast cells were cultured in liquid YEA and
 268 incubated at room temperature for 1 h with the indicated concentration of PCB (8 nM, 40 nM, 200 nM,
 269 1 μ M, 5 μ M, 25 μ M, 125 μ M, and 625 μ M). The lines and shaded areas indicate the averaged
 270 intensities and S.D., respectively (n = 50 cells). (D) Normalized absorption spectra of PCB-bound iRFP

271 (iRFP-PCB), free PCB, or iRFP. Firstly, the spectra of iRFP-PCB and iRFP were normalized based on
272 the absorbance at 280 nm (absorbance of protein), followed by the normalization of PCB spectrum by
273 the absorbance at 375 nm. (E) Normalized absorption spectra of iRFP-PCB, BV-bound iRFP (iRFP-
274 BV), and iRFP. The absorption spectra were normalized by the absorbance at 280 nm of each
275 spectrum. (F) Summary of fluorescence properties of iRFP-PCB and iRFP-BV *in vitro*. Φ and ϵ mean
276 fluorescence quantum yield and molar extinction coefficient, respectively. (G) (upper) Structure of the
277 SynPCB2.1 plasmid expressing tFnr-Fd, PcyA, and HO1. These proteins are tagged with the
278 mitochondria targeting sequence (MTS) at their N-termini and flanked by P2A, a self-cleaving peptide.
279 (lower) Quantification of iRFP fluorescence under the indicated conditions. Cells were treated with 125
280 μ M BV or PCB for 1 hr at room temperature (second and fifth columns). Each dot represents a single-
281 cell iRFP fluorescence with a boxplot, in which the box shows the quartiles of data with the whiskers
282 denoting the minimum and maximum except for the outliers detected by 1.5 times the interquartile
283 range (n = 50 cells).
284

285 **SynPCB2.1 is ideal for iRFP imaging in fission yeast**

286 For easy iRFP imaging using PCB as a chromophore, we introduced a system for efficient PCB
287 biosynthesis, SynPCB2.1, in which *tFnr-Fd*, *PcyA*, and *HO1* genes are tandemly fused with the cDNAs
288 of mitochondrial targeting sequence (MTS) at their N-termini, and flanked by self-cleaving P2A
289 peptide cDNAs for multicistronic gene expression (Uda et al., 2020) (Fig. 3H). The single-cassette of
290 SynPCB2.1 genes was knocked-in into cells expressing NLS-iRFP-NLS with pSKI vector system, and
291 expressed under *adh1* promoter. The cells expressing SynPCB2.1 showed higher iRFP fluorescence
292 than either cells treated with PCB or cells expressing three genes individually (Fig. 3H). To determine
293 whether and to what extent iRFP formed a complex with PCB or BV in the cells, we measured the
294 emission spectrum of iRFP in a living cell. As in emission spectrum *in vitro*, cells showed distinct
295 emission spectrum between iRFP-PCB and iRFP-BV, namely, blue-shifted emission spectrum of iRFP-
296 PCB (Fig. S4A). A similar shift was observed when the emission spectrum of cells expressing
297 SynPCB2.1 was compared to that of cells expressing HO1 (Fig. S4B and summarized in Fig. S4E).
298 Importantly, cells separately expressing HO1, tFnr-Fd, and PcyA exhibited an intermediate emission
299 spectrum, suggesting a mixture of iRFP-BV and iRFP-PCB in this cell line. The mixture of iRFP-BV
300 explains the reason why iRFP fluorescence by SynPCB2.1 was brighter than that generated by separate
301 expression of the three enzymes in fission yeast (Fig. 3G). Moreover, the emission spectra obtained
302 from living fission yeast cells demonstrated that iRFP-PCB was much brighter than iRFP-BV (Fig.
303 S4C and S4D). From these data, we concluded that PCB biosynthesis by SynPCB2.1 is ideal for iRFP
304 imaging in fission yeast.

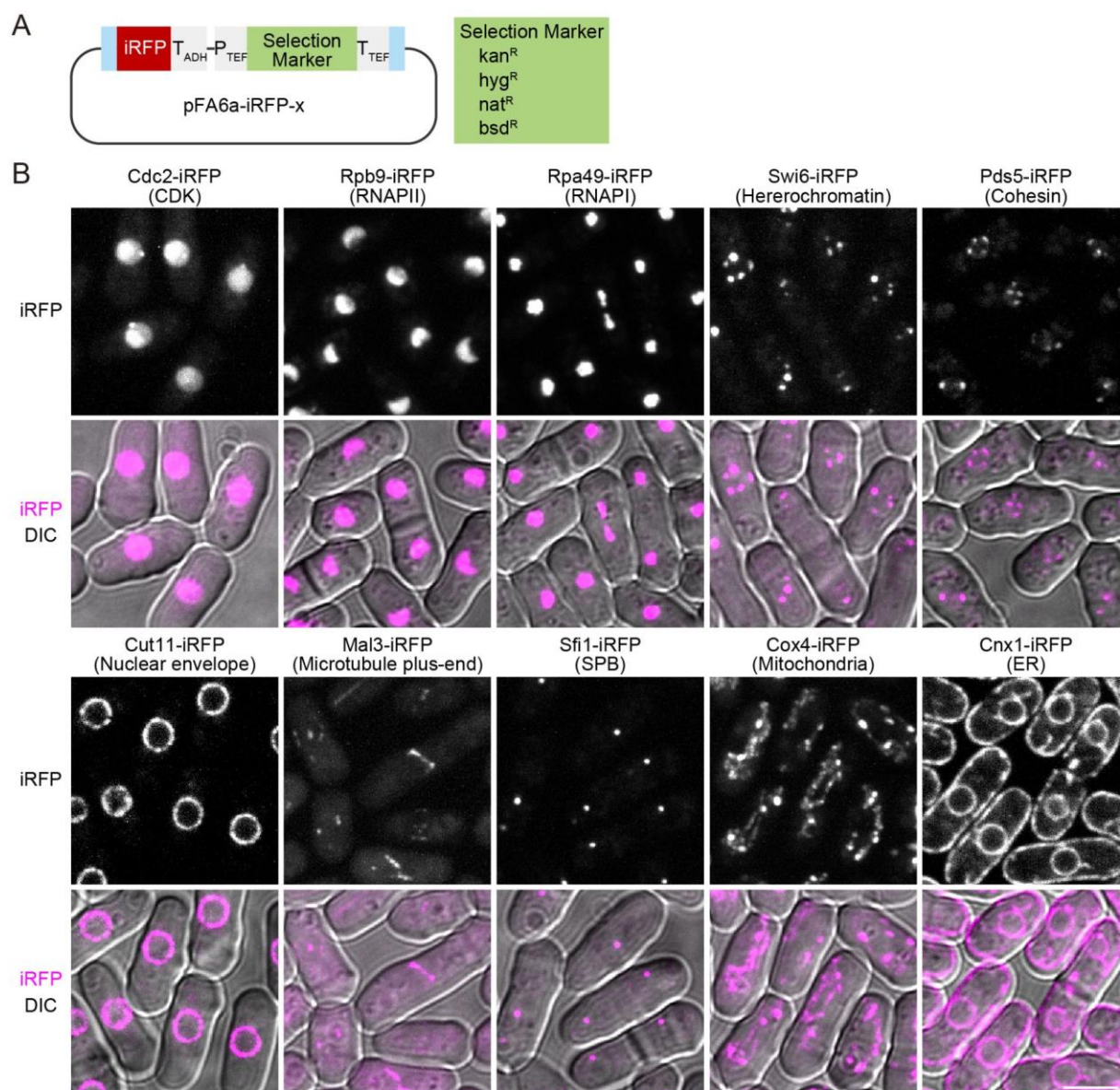
305 During iRFP imaging experiments, we found that PCB synthesized in fission yeast cells
306 expressing SynPCB2.1 is leaked out of the cells and incorporated into the surrounding cells. To clearly

307 show the PCB leakage, we co-cultured cells expressing only SynPCB2.1 and cells expressing only
308 NLS-iRFP-NLS. While both strains did not fluoresce at all, NLS-iRFP-NLS emanated fluorescence
309 when cells were co-cultured with the cells expressing SynPCB2.1 (Fig. S5B and S5C). The data
310 indicate that in fission yeast PCB is leaked into the extracellular space.

311

312 **iRFP imaging in fission yeast: Development of endogenous tagging and all-in-one integration**
313 **systems.**

314 To further exploit the advantages of iRFP imaging in fission yeast, we first established C-terminal
315 tagging plasmids based on a commonly used PCR-based tagging system (Longtine et al., 1998). The
316 plasmids include *iRFP* cassette followed by one of four different selection markers (Fig. 4A). By using
317 these plasmids, we verified endogenous *iRFP* tagging to several genes including *cdc2* (CDK, nucleus),
318 *rpb9* (PolIII, chromatin), *rpa49* (PolII, nucleolus), *swi6* (heterochromatin), *pds5* (cohesin), *cut11*
319 (nuclear envelope), *mal3* (microtubule plus-end), *sfi1* (spindle pole body, SPB), *cox4* (mitochondria),
320 and *cnx1* (endoplasmic reticulum, ER) with the expression of SynPCB2.1. All tested proteins showed
321 expected subcellular localization in fission yeast (Fig. 4B), although signal-to-noise ratios were
322 dependent on the expression level of the endogenous tagged proteins.



323

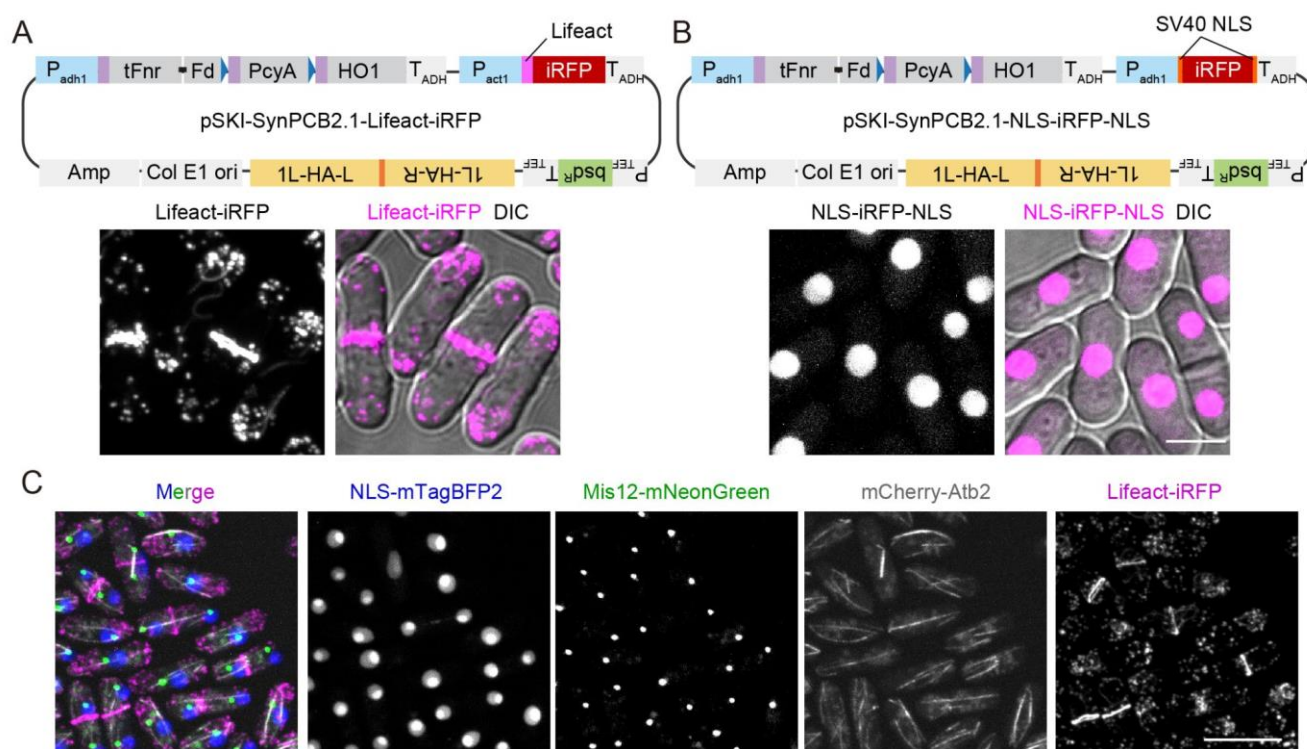
324 **Fig 4. Visualization of endogenous proteins by iRFP in fission yeast**

325 (A) Schematic illustration of the plasmid for iRFP tagging of endogenous proteins at the C-terminus.
 326 Cyan boxes indicate the common overlapping sequences (Longtine et al., 1998). The plasmid list is
 327 shown in Table S1. (B) The subcellular localization of endogenous proteins tagged with iRFP using
 328 pFA6a-iRFP. iRFP signals were shown in grayscale in upper panels, and DIC images were merged with
 329 magenta iRFP signals and shown in lower panels. Maximal projection images for iRFP are shown
 330 except for Cut11-iRFP and Cnx1-iRFP. Scale bar, 5 μ m.

331

332 Second, we developed all-in-one plasmids carrying SynPCB2.1 and iRFP fusion protein genes
 333 to avoid the issue that these two genes occupy two of the limited selection markers and integration loci.
 334 As a proof-of-concept, the cDNA of Lifeact-iRFP (F-actin marker) or NLS-iRFP-NLS (nucleus
 335 marker) is introduced into the pSKI plasmid with SynPCB2.1 gene cassette (Fig. 5A and 5B). Fission

336 yeast transformed with these plasmids displayed the bright F-actin pattern including actin patches, actin
 337 cables, and contractile ring (Fig. 5A) and nucleus (Fig. 5B). Taking full advantage of iRFP imaging
 338 with the SynPCB system in fission yeast, we established cells expressing four different proteins; the
 339 nucleus, kinetochore, tubulin, and F-actin were labeled with NLS-mTagBFP2, endogenous Mis12-
 340 mNeonGreen, mCherry-Atb2, and Lifact-iRFP, respectively (Fig. 5C).



341
 342
 343
 344
 345
 346
 347
 348
 349
 350
 351
 352

Fig 5. All-in-one plasmids for iRFP imaging.

(A) (upper) Schematic illustration of 1L locus integration plasmids for the expression of SynPCB2.1 and Lifact fused with iRFP (pSKI-SynPCB2.1-Lifact-iRFP). (lower) Representative images of fission yeast expressing Lifact-iRFP are shown with the maximal intensity projection image and DIC-merged image. (B) (upper) Schematic illustration of 1L locus integration plasmids for the expression of SynPCB2.1 and NLS-iRFP-NLS (pSKI-SynPCB2.1-NLS-iRFP-NLS). (lower) Representative images of fission yeast expressing NLS-iRFP-NLS are shown with the maximal intensity projection image and DIC-merged image. Scale bar, 5 μ m. (C) Multiplexed imaging of fission yeast expressing NLS-mTagBFP2 (nucleus), Mis12-mNeonGreen (kinetochore), mCherry-Atb2 (tubulin), and Lifact-iRFP (F-actin). Maximal intensity projection images and a merged image are shown. Scale bar 10 μ m.

PCB can be used as a chromophore in mammalian cells

354 Finally, we tested whether PCB could be used as an iRFP chromophore in other organisms. HeLa cells
 355 expressing iRFP along with EGFP, an internal control for iRFP expression, were treated with external
 356 BV or PCB. PCB treatment increased the brightness of iRFP as well as BV treatment in HeLa cells
 357 (Fig. S6A and S6B). BVRA KO HeLa cells displayed higher iRFP fluorescence than did parental HeLa

358 cells as reported previously (Kobachi et al., 2020), but did not show any change in iRFP fluorescence
359 with BV or PCB treatment (Fig. S6B), probably because all iRFP molecules were occupied by BV. In
360 contrast to fission yeast, the increment of iRFP fluorescence by PCB treatment was comparable to that
361 by BV treatment in parental HeLa cells (Fig. S6B). Taken together, we concluded that PCB is
362 applicable to iRFP imaging in mammalian cells, albeit no significant advantage over BV.
363

364 DISCUSSION

365 In this study, we demonstrated that iRFP does not fluoresce in fission yeast because of the lack of the
366 BV-producing enzyme HO. Moreover, we found that PCB acts as a brighter chromophore for iRFP
367 than BV *in vitro* and in fission yeast expressing SynPCB2.1. Although PCB is not an authentic
368 chromophore for iRFP nor original RpBphP2, our data strongly suggested that PCB forms a fluorescent
369 chromophore in iRFP. Finally, we developed endogenous iRFP tagging plasmids and all-in-one
370 plasmids carrying SynPCB2.1 and iRFP marker proteins for the easy use of near-infrared imaging in
371 fission yeast. Instead of external chromophore addition, the SynPCB2.1 system has potential
372 advantages for iRFP imaging, which are fully genetically encoded and capable of providing even
373 brighter iRFP fluorescence in fission yeast.

374 Our data indicate that PCB is more suitable for an iRFP chromophore than BV in fission yeast
375 for several reasons. First reason is the 2-fold higher fluorescence quantum yield of iRFP-PCB than that
376 of iRFP-BV *in vitro*. Second reason is that excitation and emission spectra of iRFP-PCB are blue-
377 shifted in comparison to those of iRFP-BV. This result is consistent with previous works describing the
378 blue-shifted spectra of PCB (Loughlin et al., 2016; Rumyantsev et al., 2015). The blue-shifted spectra
379 of iRFP-PCB possesses favorable properties for most of conventional confocal microscopes, which are
380 equipped with 630-640 nm excitation laser for near-infrared fluorescence imaging. Third conceivable
381 reason is the efficient chromophore formation. Indeed, RpBphP1-derived GAF-FP bound PCB 1.75-
382 fold more efficiently than BV (Rumyantsev et al., 2015). In contrast to fission yeast, HeLa cells
383 showed no difference between PCB and BV with respect to iRFP fluorescence (Fig. S6). It could be
384 partly due to the metabolism and culture condition in mammalian cells including synthesis of BV by
385 endogenous HO1, degradation of BV and PCB by BVRA (Kobachi et al., 2020; Terry et al., 1993; Uda
386 et al., 2017), and the presence of BV and bilirubin in serum of culture medium. Based on the result
387 obtained by using fission yeast, we presume that the existence of BV within a HeLa cell and in the
388 culture medium attenuates the increase in PCB-induced iRFP fluorescence. Furthermore, the other
389 tetrapyrroles, such as primarily PPIX, could compete for iRFP with BV or PCB (Lehtivuori et al.,
390 2013; Wagner et al., 2008).

391 The SynPCB system allows bright iRFP imaging without adding the external chromophores.
392 This fact lets us hypothesize the application of PCB to other BV-based fluorescent proteins and
393 optogenetic tools. Indeed, near-infrared fluorescent proteins that originate from cyanobacteriochrome
394 such as smURFP or iRFP670nano (Oliinyk et al., 2019; Rodriguez et al., 2016) exhibit high affinity to
395 PCB because the original cyanobacteriochromes bind specifically to PCB. miRFPs including

396 miRFP670, miRFP703, and miRFP720 have also been developed from bacterial phytochrome
397 RpBphP1 (Shcherbakova et al., 2016; Shemetov et al., 2017), and therefore the SynPCB systems would
398 be used for imaging with these miRFPs. Bacteriophytochrome-based optogenetic tools using BV
399 (Kaberniuk et al., 2016; Monakhov et al., 2020; Qian et al., 2020; Redchuk et al., 2017) would be a
400 potential target for the application of the SynPCB system. We should note that it is not clear whether
401 PCB, instead of BV, increases the fluorescence brightness of these near-infrared fluorescent proteins
402 and maintains the photoresponsive properties of these optogenetic tools. Fission yeast is an ideal model
403 to assess phytochrome-based tools in a cell, such as the difference between BV and PCB for
404 chromophore and the examination of genetically-encoded chromophore reconstruction, because there is
405 neither synthetic nor degradation pathway of BV in fission yeast.

406 We found that *HO* homologue is frequently lost in fungal species including the fission yeast
407 during evolution (Fig. S1). Besides fungi, *Caenorhabditis elegans*, one of the most popular model
408 organisms, has shown very low, but not zero, BV-producing activity (Ding et al., 2017). Consistently,
409 we could not find an *HO* homologue in the worm genome. The SynPCB system paves the way to
410 utilize iRFP for a broader range of organisms that lost *HO* homologue during evolution. In addition, we
411 recognized that PCB produced by SynPCB2.1 is leaked from the cells and uptaken by surrounding
412 cells, as manifested by iRFP fluorescence (Fig. S5). It is possible that the same things take place in
413 actual ecological conditions; some organisms exploit tetrapyrroles produced by other organisms in
414 order to function their own phytochromes. In fact, *Aspergillus nidulans* and *Neurospora crassa*, both of
415 which lost *HO* homologue in their genomes (Fig. S1), harbor phytochrome genes that are required for
416 chromophores (Blumenstein et al., 2005; Froehlich et al., 2005). The exchanges of tetrapyrroles
417 between living organisms might explain the reason why the *HO* gene is sporadically lost in many
418 organisms.

419 We report an iRFP imaging platform for fission yeast and the novel chromosome integration
420 plasmid series, pSKI. The endogenous iRFP tagging system is based on the commonly used one,
421 allowing anyone to introduce it quickly. The all-in-one plasmids carrying NLS-iRFP-NLS enables
422 nuclear tracking without occupying green or red color fluorescence channels and automatic analysis of
423 large-scale time-lapse images with nuclear translocation type sensors (Regot et al., 2014). Further
424 characterization and engineering will result in wide use of iRFP and phytochrome-based optogenetic
425 tools in living organisms.

426

427 MATERIALS AND METHODS

428

429 Plasmids

430 The cDNAs of *PcyA*, *HO1*, *Fd*, and *Fnr* were originally derived from *Thermosynechococcus elongatus*
431 BP-1 as previously described (Uda et al., 2020). The mitochondrial targeting sequence (MTS;
432 MSVLTPLLLRGLTGSARRLP) was derived from human cytochrome C oxidase subunit VIII. The
433 cDNAs were subcloned into vectors through conventional ligation with Ligation high Ver.2 (Toyobo,
434 Osaka, Japan) or NEBuilder HiFi DNA Assembly (New England Biolabs, Ipswich, MA) according to
435 the manufacturers' instruction. The nucleotide sequence of mNeonGreen was optimized for fission
436 yeast codon usage (see Benchling link, Table S1). pSKI vectors include *Amp*, *colEI ori* (derived from
437 pUC119), selection marker cassettes (derived from pFA6a-3FLAG-bsd, pFA6a-kan, pAV0587
438 (pHis5Stul-bleMX), pMNATZA1, and pHBCN1), *Padh1*, *Tadh1* (derived from pNATZA1), *Pnmt1*,
439 *Tnmt1* (derived from pREP1), and MCSs (synthesized as oligo DNA (Fasmac)). To construct pSKI-
440 SynPCB2.1-Lifeact-iRFP, *Pact1* (822 bp upstream of the start codon) was cloned from the fission yeast
441 genome, and the cDNA of Lifeact was introduced by ligating annealed oligo DNAs. All plasmids used
442 in this study are listed in Table S1 with Benchling links, which include the sequences and plasmid
443 maps.

444

445 Reagents

446 Biliverdin hydrochloride was purchased from Sigma-Aldrich (30891-50MG), dissolved in DMSO (25
447 mM stock solution and final concentration ranged from 8 nM to 625 μ M), and stored at -30°C . PCB
448 was purchased from Santa Cruz Biotechnology (sc-396921), dissolved in DMSO (final concentration, 5
449 mM), and stored at -30°C .

450

451 Fission yeast *Schizosaccharomyces pombe* strain and culture

452 All strains made and used in this study are listed in Table S2. The growth medium, sporulation
453 medium, and other techniques for fission yeast were based on the protocol described previously
454 (Moreno et al., 1991) unless otherwise noted. Transformation protocol was modified from (Suga and
455 Hatakeyama, 2005). Genome integration by pSKI was confirmed by colony PCR with KOD One
456 (TOYOBO) and primers listed in Table S3. For the fluorescence microscope imaging, the fission yeast
457 cells were concentrated by centrifugation at 3,000 rpm, mounted on a slide glass, and sealed by a cover
458 glass (Matsunami).

459

460 **HeLa cell culture**

461 HeLa cells were gifted from Michiyuki Matsuda (Kyoto University) and cultured in Dulbecco's
462 Modified Eagle's Medium (DMEM) high glucose (Wako; nacalai tesque) supplemented with 10% fetal
463 bovine serum (FBS) (Sigma-Aldrich) at 37°C in 5% CO₂. For the live-cell imaging, HeLa cells were
464 plated on CELLview cell culture dishes (glass bottom, 35 mm diameter, 4 components: The Greiner
465 Bio-One). One day after seeding, transfection was performed with 293fectin transfection reagent
466 (Thermo Fisher Scientific). Two days after transfection, cells were imaged with fluorescence
467 microscopes. BV or PCB was added into the DMEM medium containing 10% FBS for 3 h at 37°C in
468 5% CO₂.

469

470 **Measurement of the growth rate of fission yeast**

471 Fission yeast cells were pre-cultured at 30 °C up to the optical density at 600 nm (OD600) of 1.0,
472 followed by dilution to 1:100. A Compact Rocking Incubator Biophotorecorder TVS062CA (Advantec,
473 Japan) was used for culture growth (30 °C, 70 rpm) and OD660 measurement. Growth curves were
474 fitted by the logistic function ($x = K / (1 + (K/x_0 - 1)e^{-rt})$) and doubling time ($\ln 2 / r$) was calculated on
475 Python 3 and Scipy.

476

477 **Protein purification**

478 For the purification of His-tag fused iRFP, pCold-TEV-linker-iRFP was transformed into BL21(DE3)
479 pLysS. *E. coli* (Promega, L1195) and selected on LB plates containing 0.1 mg/ml ampicillin at 37°C
480 overnight. A single colony was picked up and inoculated into 2.5 mL liquid LB medium supplemented
481 with 0.1 mg/ml ampicillin and 30 µg/ml chloramphenicol at 37°C overnight. Preculture was further
482 inoculated into 250 mL liquid LB medium (1:100) containing ampicillin and chloramphenicol. The
483 culture was shaken at 37°C for 2-4 h until OD600 reached 0.6-1.0. The culture was shifted to 18°C with
484 the addition of 0.25 mM Isopropyl β-D-1-thiogalactopyranoside (IPTG) (Wako, 094-05144) to induce
485 the expression of His fused protein. After the overnight incubation at 18°C, cells were collected and
486 suspended into phosphate buffer saline (PBS) (Takara, T900) containing 20 mM imidazole (Nacalai
487 tesque, 19004-22). Suspended cells were lysed by the sonication (VP-300N, TAITEC), followed by
488 centrifugation to collect the supernatant. The supernatant was mixed with 250 µL Ni-NTA sepharose
489 (Qiagen, 1018244), and incubated at 4°C for 2 h. Protein-bound beads were washed with PBS
490 containing 20 mM imidazole, and proteins were eluted by the addition of 300 mM imidazole in PBS.

491 Eluted fractions were checked by SDS-PAGE with a protein molecular weight marker Precision Plus
492 ProteinTM All Blue Standards (Bio-Rad, #1610373) followed by CBB staining (BIOCRAFT, CBB-
493 250), detected by Odyssey CLx (Licor). Protein-containing fractions were dialyzed using Slide-A-
494 Lyzer Dialysis Cassette 3,500 MWCO (Thermo Scientific, 66110) to remove the imidazole. To
495 concentrate the recombinant protein, amicon ultra 3K 500 μ L (Millipore, UFC500308) was used.
496 Purified His-iRFP was mixed with an excess amount of BV or PCB (1:5 molar ratio), followed by the
497 size exclusion chromatography with NAP-5 Columns (Cytiva, 17085301) to remove free BV or PCB.

498

499 **Characterization of *in vitro* fluorescence properties**

500 The absorption of BV (100 μ M), PCB (100 μ M), and His-iRFP (12 μ M) bound to chromophore was
501 measured by nanophotometer P330 (IMPLEN) with 10 mm quartz glass cuvette (TOSOH, T-29M
502 UV10). The absorption spectrum was measured in a wavelength range of 200 nm to 950 nm. For the
503 measurements of absolute fluorescence quantum yield, BV or PCB bound His-iRFP (1 μ M) in PBS
504 were subjected to Quantaurus-QY C11347-01 (HAMAMATSU PHOTONICS). The excitation
505 wavelength was 640 nm. For the measurements of excitation and emission spectra, BV or PCB bound
506 His-iRFP (12 μ M) were subjected to Fluorescence Spectrophotometer F-4500 (HITACHI). The protein
507 solution was excited in a wavelength range of 500 nm to 720 nm and fluorescence at 730 nm was
508 detected to measure the excitation spectrum. To measure the emission spectrum, the protein solution
509 was excited at 640 nm, and fluorescence was detected in a wavelength range of 660 nm to 800 nm.

510

511 **Measurement of *in vivo* emission spectrum**

512 The lambda-scan function of Leica SP8 Falcon was used for the measurement of the fluorescence
513 emission spectrum. The excitation wavelength was fixed at 633 nm, and the 20 nm emission window
514 was slid in 3 nm increment from 650 nm to 768 nm. Each emission spectrum was normalized by the
515 peak emission value.

516

517 **Live-cell fluorescence imaging**

518 Cells were imaged with an IX83 inverted microscope (Olympus) equipped with an sCMOS camera
519 (ORCA-Fusion BT, Hamamatsu Photonics), an oil objective lens (UPLXAPO 100X, NA = 1.45, WD =
520 0.13 mm or UPLXAPO 60X, NA = 1.42, WD = 0.15 mm; Olympus), and a spinning disk confocal unit
521 (CSU-W1, Yokogawa Electric Corporation). The excitation laser and fluorescence filter settings were
522 as follows: Excitation laser, 445 nm, 488 nm, 561 nm, and 640 nm for mTagBFP2, mNeonGreen (or

523 EGFP), mCherry, and iRFP, respectively; excitation dichroic mirror, DM445/514/640 (Yokogawa
524 Electric) for mTagBFP2, and DM405/488/561/640 for others; emission filters, 482/35 for mTagBFP2,
525 525/50 for mNeonGreen or EGFP, 617/73 for mCherry, and 685/40 for iRFP (Yokogawa Electric)

526

527 **Imaging analysis**

528 All fluorescence imaging data were analyzed and quantified by Fiji (Image J). The background was
529 subtracted by the rolling-ball method. Some images were obtained with 10-30 Z-slices of 0.2 μm
530 interval and shown as 2D images by the maximal intensity projection as noted in each figure legend.
531 For the quantification of signal intensity, appropriate ROIs were manually selected, and mean
532 intensities in ROIs were measured.

533

534 **Analysis of *HO*-like sequences in fungal species**

535 We searched for *HO*-like sequences in representative fungal species using BLASTp (See Table S4 for
536 the details). We adopted human *HO1* (Uniprot P09601) and *S. cerevisiae* *HMX1* (Uniprot P32339) as
537 the queries (e-value < 1e-5). The phylogenetic relationship is based on recent studies using multiple
538 genes (Li et al., 2021; Nguyen et al., 2017). Since the results suggested sequence divergence among
539 *HO1* homologues, we also used *HO*-like proteins of *Laccaria bicolor* and *Saitoella complicata*
540 obtained from the BLASTp hits, although no additional sequence was found. Note that the absence in
541 *Aspergillus nidulans* and the existence in *Candida albicans* are consistent with previous studies
542 (Blumenstein et al., 2005; Pendrak et al., 2004). Concerning *C. elegans*, we searched for *HO-like*
543 *sequence* by the BLASTp interface provided on the WormBase web site (<http://www.wormbase.org>,
544 release WS280, date 20-Dec-2020, database version WS279). We used the same protein queries, *i.e.*,
545 human *HO1* and *S. cerevisiae* *HMX1*, although we obtained no-hit (e-value < 1e-2).

546

547 **Acknowledgments**

548 We thank all members of the Aoki Laboratory for their helpful discussions and assistance. The
549 pCold-TEV plasmid was gifted from Dr. Koichi Kato (ExCELLS). Some fission yeast strains were
550 provided by the National Bio-Resource Project (NBRP), Japan. We thank the Functional Genomics
551 Facility, NIBB Core Research Facilities for fluorescence spectrometry technical support.

552

553 **Competing Interests**

554 The authors declare no competing or financial interest.

555

556 **Author contributions**

557 Conceptualization: Y.G.; Data curation: Y.G., K.S., Y.K.; Formal analysis: Y.G., K.S., Y.K.;
558 Funding acquisition: Y.K., M.K., Y.G., K.A.; Investigation: Y.G., K.S., Y.K., H.F, M.K.;
559 Methodology: Y.G., K.S., Y.K., H.F, M.K.; Project administration: Y.G., K.A.; Resources: Y.G., K.S.,
560 H.F, M.K.; Supervision: K.A., Y.G.; Visualization: Y.G., K.S., Y.K.; Validation: Y.G., K.S., Y.K.;
561 Writing - original draft: Y.G., K.S., Y.K., K.A.; Writing - review & editing: Y.G., K.S., Y.K., K.A..

562

563 **Funding**

564 K.A. was supported by a CREST, JST Grant (JPMJCR1654), JSPS KAKENHI Grants (nos.
565 18H02444, and 19H05798), and the ONO Medical Research Foundation. Y.G. was supported by a
566 JSPS KAKENHI Grant (no.19K16050), a Jigami Yoshifumi Memorial Research Grant, and a
567 Sumitomo Research grant. Y.K. was supported by JSPS KAKENHI Grants (nos. 19K16207 and
568 19H05675).

569

570 **References**

- 571 **Blumenstein, A., Vienken, K., Tasler, R., Purschwitz, J., Veith, D., Frankenberg-Dinkel, N. and**
572 **Fischer, R.** (2005). The *Aspergillus nidulans* phytochrome FphA represses sexual development in
573 red light. *Curr. Biol.* **15**, 1833–1838.
- 574 **Chernov, K. G., Redchuk, T. A., Omelina, E. S. and Verkhusha, V. V.** (2017). Near-Infrared
575 Fluorescent Proteins, Biosensors, and Optogenetic Tools Engineered from Phytochromes. *Chem.*
576 *Rev.* **117**, 6423–6446.
- 577 **Ding, W.-L., Miao, D., Hou, Y.-N., Jiang, S.-P., Zhao, B.-Q., Zhou, M., Scheer, H. and Zhao, K.-**
578 **H.** (2017). Small monomeric and highly stable near-infrared fluorescent markers derived from the
579 thermophilic phycobiliprotein, ApcF2. *Biochim. Biophys. Acta Mol. Cell Res.* **1864**, 1877–1886.
- 580 **Fennessy, D., Grallert, A., Krapp, A., Cokoja, A., Bridge, A. J., Petersen, J., Patel, A., Tallada, V.**
581 **A., Boke, E., Hodgson, B., et al.** (2014). Extending the *Schizosaccharomyces pombe* molecular
582 genetic toolbox. *PLoS One* **9**, e97683.
- 583 **Filonov, G. S., Piatkevich, K. D., Ting, L.-M., Zhang, J., Kim, K. and Verkhusha, V. V.** (2011).
584 Bright and stable near-infrared fluorescent protein for in vivo imaging. *Nat. Biotechnol.* **29**, 757–
585 761.
- 586 **Froehlich, A. C., Noh, B., Vierstra, R. D., Loros, J. and Dunlap, J. C.** (2005). Genetic and
587 molecular analysis of phytochromes from the filamentous fungus *Neurospora crassa*. *Eukaryot.*
588 *Cell* **4**, 2140–2152.
- 589 **Fushimi, K. and Narikawa, R.** (2021). Phytochromes and Cyanobacteriochromes: Photoreceptor
590 Molecules Incorporating a Linear Tetrapyrrole Chromophore. In *Optogenetics: Light-Sensing*
591 *Proteins and Their Applications in Neuroscience and Beyond* (ed. Yawo, H.), Kandori, H.),
592 Koizumi, A.), and Kageyama, R.), pp. 167–187. Singapore: Springer Singapore.
- 593 **Fushimi, K., Miyazaki, T., Kuwasaki, Y., Nakajima, T., Yamamoto, T., Suzuki, K., Ueda, Y.,**
594 **Miyake, K., Takeda, Y., Choi, J.-H., et al.** (2019). Rational conversion of chromophore
595 selectivity of cyanobacteriochromes to accept mammalian intrinsic biliverdin. *Proc. Natl. Acad.*
596 *Sci. U. S. A.* **116**, 8301–8309.
- 597 **Gambetta, G. A. and Lagarias, J. C.** (2001). Genetic engineering of phytochrome biosynthesis in
598 bacteria. *Proc. Natl. Acad. Sci. U. S. A.* **98**, 10566–10571.
- 599 **Geller, S. H., Antwi, E. B., Di Ventura, B. and McClean, M. N.** (2019). Optogenetic Repressors of
600 Gene Expression in Yeasts Using Light-Controlled Nuclear Localization. *Cell. Mol. Bioeng.* **12**,
601 511–528.
- 602 **Hochrein, L., Machens, F., Messerschmidt, K. and Mueller-Roeber, B.** (2017). PhiReX: a
603 programmable and red light-regulated protein expression switch for yeast. *Nucleic Acids Res.* **45**,
604 9193–9205.
- 605 **Kaberniuk, A. A., Shemetov, A. A. and Verkhusha, V. V.** (2016). A bacterial phytochrome-based
606 optogenetic system controllable with near-infrared light. *Nat. Methods* **13**, 591–597.

- 607 **Kakui, Y., Sunaga, T., Arai, K., Dodgson, J., Ji, L., Csikász-Nagy, A., Carazo-Salas, R. and Sato,**
608 **M.** (2015). Module-based construction of plasmids for chromosomal integration of the fission
609 yeast *Schizosaccharomyces pombe*. *Open Biol.* **5**, 150054.
- 610 **Kamper, M., Ta, H., Jensen, N. A., Hell, S. W. and Jakobs, S.** (2018). Near-infrared STED
611 nanoscopy with an engineered bacterial phytochrome. *Nat. Commun.* **9**, 4762.
- 612 **Keeney, J. B. and Boeke, J. D.** (1994). Efficient targeted integration at *leu1-32* and *ura4-294* in
613 *Schizosaccharomyces pombe*. *Genetics* **136**, 849–856.
- 614 **Kobachi, K., Kuno, S., Sato, S., Sumiyama, K., Matsuda, M. and Terai, K.** (2020). Biliverdin
615 Reductase-A Deficiency Brighten and Sensitize Biliverdin-binding Chromoproteins. *Cell Struct.*
616 *Funct.* **45**, 131–141.
- 617 **Kyriakakis, P., Catanho, M., Hoffner, N., Thavarajah, W., Hu, V. J., Chao, S.-S., Hsu, A., Pham,**
618 **V., Naghavian, L., Dozier, L. E., et al.** (2018). Biosynthesis of Orthogonal Molecules Using
619 Ferredoxin and Ferredoxin-NADP⁺ Reductase Systems Enables Genetically Encoded PhyB
620 Optogenetics. *ACS Synth. Biol.* **7**, 706–717.
- 621 **Lambert, T. J.** (2019). FPbase: a community-editable fluorescent protein database. *Nat. Methods* **16**,
622 277–278.
- 623 **Landgraf, F. T., Forreiter, C., Hurtado Picó, A., Lamparter, T. and Hughes, J.** (2001).
624 Recombinant holophytochrome in *Escherichia coli*. *FEBS Lett.* **508**, 459–462.
- 625 **Lehtivuori, H., Rissanen, I., Takala, H., Bamford, J., Tkachenko, N. V. and Ihalainen, J. A.**
626 (2013). Fluorescence properties of the chromophore-binding domain of bacteriophytochrome from
627 *Deinococcus radiodurans*. *J. Phys. Chem. B* **117**, 11049–11057.
- 628 **Li, Y., Jin, M., O’Laughlin, R., Bittihn, P., Tsimring, L. S., Pillus, L., Hasty, J. and Hao, N.**
629 (2017). Multigenerational silencing dynamics control cell aging. *Proc. Natl. Acad. Sci. U. S. A.*
630 **114**, 11253–11258.
- 631 **Li, Y., Steenwyk, J. L., Chang, Y., Wang, Y., James, T. Y., Stajich, J. E., Spatafora, J. W.,**
632 **Groenewald, M., Dunn, C. W., Hittinger, C. T., et al.** (2021). A genome-scale phylogeny of the
633 kingdom Fungi. *Curr. Biol.* **31**, 1653–1665.e5.
- 634 **Longtine, M. S., McKenzie, A., 3rd, Demarini, D. J., Shah, N. G., Wach, A., Brachat, A.,**
635 **Philippsen, P. and Pringle, J. R.** (1998). Additional modules for versatile and economical PCR-
636 based gene deletion and modification in *Saccharomyces cerevisiae*. *Yeast* **14**, 953–961.
- 637 **Loughlin, P. C., Duxbury, Z., Mugerwa, T. T. M., Smith, P. M. C., Willows, R. D. and Chen, M.**
638 (2016). Spectral properties of bacteriophytochrome AM1_5894 in the chlorophyll d-containing
639 cyanobacterium *Acaryochloris marina*. *Sci. Rep.* **6**, 27547.
- 640 **Matlashov, M. E., Shcherbakova, D. M., Alvelid, J., Baloban, M., Pennacchietti, F., Shemetov, A.**
641 **A., Testa, I. and Verkhusha, V. V.** (2020). A set of monomeric near-infrared fluorescent proteins
642 for multicolor imaging across scales. *Nat. Commun.* **11**, 239.

- 643 **Matsuyama, A., Shirai, A., Yashiroda, Y., Kamata, A., Horinouchi, S. and Yoshida, M.** (2004).
644 pDUAL, a multipurpose, multicopy vector capable of chromosomal integration in fission yeast.
645 *Yeast* **21**, 1289–1305.
- 646 **Maundrell, K.** (1993). Thiamine-repressible expression vectors pREP and pRIP for fission yeast. *Gene*
647 **123**, 127–130.
- 648 **Monakhov, M. V., Matlashov, M. E., Colavita, M., Song, C., Shcherbakova, D. M., Antic, S. D.,**
649 **Verkhusha, V. V. and Knöpfel, T.** (2020). Screening and Cellular Characterization of
650 Genetically Encoded Voltage Indicators Based on Near-Infrared Fluorescent Proteins. *ACS Chem.*
651 *Neurosci.* **11**, 3523–3531.
- 652 **Moreno, S., Klar, A. and Nurse, P.** (1991). Molecular genetic analysis of fission yeast
653 *Schizosaccharomyces pombe*. *Methods Enzymol.* **194**, 795–823.
- 654 **Mukougawa, K., Kanamoto, H., Kobayashi, T., Yokota, A. and Kohchi, T.** (2006). Metabolic
655 engineering to produce phytochromes with phytochromobilin, phycocyanobilin, or
656 phycoerythrobilin chromophore in *Escherichia coli*. *FEBS Lett.* **580**, 1333–1338.
- 657 **Müller, K., Engesser, R., Timmer, J., Nagy, F., Zurbriggen, M. D. and Weber, W.** (2013).
658 Synthesis of phycocyanobilin in mammalian cells. *Chem. Commun.* **49**, 8970–8972.
- 659 **Nguyen, T. A., Cissé, O. H., Yun Wong, J., Zheng, P., Hewitt, D., Nowrousian, M., Stajich, J. E.**
660 **and Jedd, G.** (2017). Innovation and constraint leading to complex multicellularity in the
661 Ascomycota. *Nat. Commun.* **8**, 14444.
- 662 **Oliinyk, O. S., Shemetov, A. A., Pletnev, S., Shcherbakova, D. M. and Verkhusha, V. V.** (2019).
663 Smallest near-infrared fluorescent protein evolved from cyanobacteriochrome as versatile tag for
664 spectral multiplexing. *Nat. Commun.* **10**, 279.
- 665 **Pendrak, M. L., Chao, M. P., Yan, S. S. and Roberts, D. D.** (2004). Heme Oxygenase in *Candida*
666 *albicans* Is Regulated by Hemoglobin and Is Necessary for Metabolism of Exogenous Heme and
667 Hemoglobin to α -Biliverdin*. *J. Biol. Chem.* **279**, 3426–3433.
- 668 **Piatkevich, K. D., Suk, H.-J., Kodandaramaiah, S. B., Yoshida, F., DeGennaro, E. M., Drobizhev,**
669 **M., Hughes, T. E., Desimone, R., Boyden, E. S. and Verkhusha, V. V.** (2017). Near-Infrared
670 Fluorescent Proteins Engineered from Bacterial Phytochromes in Neuroimaging. *Biophys. J.* **113**,
671 2299–2309.
- 672 **Qian, Y., Cosio, D. M. O., Piatkevich, K. D., Aufmkolk, S., Su, W.-C., Celiker, O. T., Schohl, A.,**
673 **Murdock, M. H., Aggarwal, A., Chang, Y.-F., et al.** (2020). Improved genetically encoded near-
674 infrared fluorescent calcium ion indicators for in vivo imaging. *PLoS Biol.* **18**, e3000965.
- 675 **Redchuk, T. A., Omelina, E. S., Chernov, K. G. and Verkhusha, V. V.** (2017). Near-infrared
676 optogenetic pair for protein regulation and spectral multiplexing. *Nat. Chem. Biol.* **13**, 633–639.
- 677 **Regot, S., Hughey, J. J., Bajar, B. T., Carrasco, S. and Covert, M. W.** (2014). High-sensitivity
678 measurements of multiple kinase activities in live single cells. *Cell* **157**, 1724–1734.

- 679 **Rhie, G. and Beale, S. I.** (1992). Biosynthesis of phycobilins. Ferredoxin-supported nadph-
680 independent heme oxygenase and phycobilin-forming activities from *Cyanidium caldarium*. *J.*
681 *Biol. Chem.* **267**, 16088–16093.
- 682 **Rodriguez, E. A., Tran, G. N., Gross, L. A., Crisp, J. L., Shu, X., Lin, J. Y. and Tsien, R. Y.**
683 (2016). A far-red fluorescent protein evolved from a cyanobacterial phycobiliprotein. *Nat.*
684 *Methods* **13**, 763–769.
- 685 **Rogers, O. C., Johnson, D. M. and Firnberg, E.** (2019). mRhubarb: Engineering of monomeric, red-
686 shifted, and brighter variants of iRFP using structure-guided multi-site mutagenesis. *Sci. Rep.* **9**,
687 15653.
- 688 **Rumyantsev, K. A., Shcherbakova, D. M., Zakharova, N. I., Emelyanov, A. V., Turoverov, K. K.**
689 **and Verkhusha, V. V.** (2015). Minimal domain of bacterial phytochrome required for
690 chromophore binding and fluorescence. *Sci. Rep.* **5**, 18348.
- 691 **Shcherbakova, D. M. and Verkhusha, V. V.** (2013). Near-infrared fluorescent proteins for multicolor
692 in vivo imaging. *Nat. Methods* **10**, 751–754.
- 693 **Shcherbakova, D. M., Baloban, M., Emelyanov, A. V., Brenowitz, M., Guo, P. and Verkhusha, V.**
694 **V.** (2016). Bright monomeric near-infrared fluorescent proteins as tags and biosensors for
695 multiscale imaging. *Nat. Commun.* **7**, 12405.
- 696 **Shcherbakova, D. M., Cox Cammer, N., Huisman, T. M., Verkhusha, V. V. and Hodgson, L.**
697 (2018). Direct multiplex imaging and optogenetics of Rho GTPases enabled by near-infrared
698 FRET. *Nat. Chem. Biol.* **14**, 591–600.
- 699 **Shemetov, A. A., Oliinyk, O. S. and Verkhusha, V. V.** (2017). How to Increase Brightness of Near-
700 Infrared Fluorescent Proteins in Mammalian Cells. *Cell Chem Biol* **24**, 758–766.e3.
- 701 **Shin, A.-Y., Han, Y.-J., Song, P.-S. and Kim, J.-I.** (2014). Expression of recombinant full-length
702 plant phytochromes assembled with phytochromobilin in *Pichia pastoris*. *FEBS Lett.* **588**, 2964–
703 2970.
- 704 **Siam, R., Dolan, W. P. and Forsburg, S. L.** (2004). Choosing and using *Schizosaccharomyces pombe*
705 plasmids. *Methods* **33**, 189–198.
- 706 **Stepanenko, O. V., Baloban, M., Bublikov, G. S., Shcherbakova, D. M., Stepanenko, O. V.,**
707 **Turoverov, K. K., Kuznetsova, I. M. and Verkhusha, V. V.** (2016). Allosteric effects of
708 chromophore interaction with dimeric near-infrared fluorescent proteins engineered from bacterial
709 phytochromes. *Sci. Rep.* **6**, 18750.
- 710 **Suga, M. and Hatakeyama, T.** (2005). A rapid and simple procedure for high-efficiency lithium
711 acetate transformation of cryopreserved *Schizosaccharomyces pombe* cells. 799–804.
- 712 **Terry, M. J., Maines, M. D. and Lagarias, J. C.** (1993). Inactivation of phytochrome- and
713 phycobiliprotein-chromophore precursors by rat liver biliverdin reductase. *J. Biol. Chem.* **268**,
714 26099–26106.

- 715 **Tojima, T., Suda, Y., Ishii, M., Kurokawa, K. and Nakano, A.** (2019). Spatiotemporal dissection of
716 the trans-Golgi network in budding yeast. *J. Cell Sci.* **132**,.
- 717 **Tooley, A. J., Cai, Y. A. and Glazer, A. N.** (2001). Biosynthesis of a fluorescent cyanobacterial C-
718 phyocyanin holo- α subunit in a heterologous host. *Proc. Natl. Acad. Sci. U. S. A.* **98**, 10560–
719 10565.
- 720 **Uda, Y., Goto, Y., Oda, S., Kohchi, T., Matsuda, M. and Aoki, K.** (2017). Efficient synthesis of
721 phyocyanobilin in mammalian cells for optogenetic control of cell signaling. *Proc. Natl. Acad.*
722 *Sci. U. S. A.* **114**, 11962–11967.
- 723 **Uda, Y., Miura, H., Goto, Y., Yamamoto, K., Mii, Y., Kondo, Y., Takada, S. and Aoki, K.** (2020).
724 Improvement of Phyocyanobilin Synthesis for Genetically Encoded Phytochrome-Based
725 Optogenetics. *ACS Chem. Biol.*
- 726 **Vještica, A., Marek, M., Nkosi, P. J., Merlini, L., Liu, G., Bérard, M., Billault-Chaumartin, I. and**
727 **Martin, S. G.** (2020). A toolbox of stable integration vectors in the fission yeast
728 *Schizosaccharomyces pombe*. *J. Cell Sci.* **133**,.
- 729 **Wagner, J. R., Zhang, J., von Stetten, D., Günther, M., Murgida, D. H., Mroginski, M. A.,**
730 **Walker, J. M., Forest, K. T., Hildebrandt, P. and Vierstra, R. D.** (2008). Mutational analysis
731 of *Deinococcus radiodurans* bacteriophytochrome reveals key amino acids necessary for the
732 photochromicity and proton exchange cycle of phytochromes. *J. Biol. Chem.* **283**, 12212–12226.
- 733 **Wosika, V., Durandau, E., Varidel, C., Aymoz, D., Schmitt, M. and Pelet, S.** (2016). New families
734 of single integration vectors and gene tagging plasmids for genetic manipulations in budding
735 yeast. *Mol. Genet. Genomics* **291**, 2231–2240.
- 736 **Yu, D., Gustafson, W. C., Han, C., Lafaye, C., Noirclerc-Savoie, M., Ge, W.-P., Thayer, D. A.,**
737 **Huang, H., Kornberg, T. B., Royant, A., et al.** (2014). An improved monomeric infrared
738 fluorescent protein for neuronal and tumour brain imaging. *Nat. Commun.* **5**, 3626.
- 739 **Yu, D., Baird, M. A., Allen, J. R., Howe, E. S., Klassen, M. P., Reade, A., Makhijani, K., Song, Y.,**
740 **Liu, S., Murthy, Z., et al.** (2015). A naturally monomeric infrared fluorescent protein for protein
741 labeling in vivo. *Nat. Methods* **12**, 763–765.

742